Journal of Materials Chemistry C

PAPER

View Article Online
View Journal | View Issue

Cite this: J. Mater. Chem. C, 2014, 2, 7823

A novel, warm, white light-emitting phosphor $Ca_2PO_4Cl:Eu^{2+}$, Mn^{2+} for white LEDs†

Panlai Li,* Zhijun Wang,* Zhiping Yang and Qinglin Guo

A series of single-phase phosphors, $Ca_2PO_4Cl:Eu^{2+}$, Mn^{2+}, have been successfully synthesized by a solid-state method and their photoluminescence properties have been investigated. $Ca_2PO_4Cl:Eu^{2+}$, Mn^{2+} can be excited at wavelengths between 250 and 450 nm, which is within the range of the ultraviolet light-emitting diode (LED). As a result of fine tuning the emission composition of Eu^{2+} and Mn^{2+} ions, warm white light can be realized by combining the emission in a single host lattice under excitation by ultraviolet light. Efficient resonant energy transfer from Eu^{2+} to Mn^{2+} ions has been demonstrated to be a dipole–quadrupole mechanism in Ca_2PO_4Cl, and the energy transfer efficiency increases with increasing Mn^{2+} concentration, confirmed by luminescence spectra and fluorescence decay times. The energy transfer efficiency and critical distance have also been calculated. A warm, white LED has been fabricated using the single-phase white-emitting phosphor, $Ca_2PO_4Cl:0.07Eu^{2+}$, $0.2Mn^{2+}$, pumped by a 400 nm LED chip. Our results give CIE chromaticity coordinates for the white LEDs as (0.3102, 0.3096), and a correlated color temperature of 4296 K. $Ca_2PO_4Cl:Eu^{2+}$, Mn^{2+} is therefore able to serve as a potential, warm, white emitting material for white LEDs.

Received 21st May 2014
Accepted 27th July 2014

DOI: 10.1039/c4tc01055h

www.rsc.org/MaterialsC

1. Introduction

In recent years white light-emitting diodes (LEDs) have become important solid-state light sources because of their combination of high brightness, low power consumption and long duration.[1–3] However, white LEDs based on a 460 nm blue chip + YAG:Ce^{3+} phosphor merely exhibit a high correlated color temperature (CCT ≈ 7750 K) with a poor color rendering index (CRI ≈ 70–80), because of the lack of a red component.[4] Recently, white LEDs fabricated using a near ultraviolet (*n*-UV) LED coupled with red, green and blue phosphors have attracted considerable attention.[5] Furthermore, the phosphors display different rates of light output degradation, giving an unstable white light, and there is a trade-off in luminous efficiency attributable to reabsorption. The design of a single-phase phosphor pumped by UV chips, is therefore, of significance for white LEDs, since this phosphor would have the advantage of excellent color rendering indexes, with an electro-optical design for controlling different colors which is simpler than using mixed phosphors.[6–8]

A number of single-phase, white light emitting phosphors suitable for UV-pumped white LEDs have been reported.[9–11] Some single-doped examples, such as those doped with Eu^{3+}, can also produce white light,[12] but most phosphors produce white light by energy transfer within the same compound from a sensitizer to an activator, giving better color rendering and a lower CCT, in the region of 5000–7500 K, including Ce^{3+}/Eu^{2+} and Eu^{2+}/Mn^{2+} co-doped phosphors.[13–15] In addition, $Eu^{2+}/Tb^{3+}/Mn^{2+}$ or $Ce^{3+}/Tb^{3+}/Mn^{2+}$ tri-activated phosphors can also emit white light, with a higher CRI and a lower CCT (approximately 6500 K).[16–20] Warm white light suitable for indoor illumination, similar to that obtained with most luminescence lamps, has a low CCT (below 4500 K, or ideally 3500 K). This is preferable for human sight and is, therefore, recommended. Unfortunately the reported results seldom create warm, white light suitable for indoor applications,[21–23] and there is an urgent need for a single-phase warm, white light emitting phosphor with a lower CCT and excellent luminescence.

It is well known that Eu^{2+} is of great interest because its d–f emission is partly allowed, resulting in high emission intensity.[24] Emission energy is strongly dependent on crystal field and covalency, and Eu^{2+}-doped phosphors usually produce strong absorption in the UV and visible region, and exhibit a broad emission band covering the color range from blue to red.[25] Generally speaking, the emitting materials comprise an activator and a host, in which the choice of host is the key to efficient emission. Halide containing oxides are good candidates as host structures and offer a number of advantages, such as low synthesis temperature and high chemical and physical stability, and they exhibit interesting luminescence when doped with Eu^{2+}. Examples include $Ca_{12}Al_{14}O_{33}Cl_2$, $Ca_2Al_3O_6F$, Ca_2LiSiO_4F, $La_6Ba_4(SiO_4)_6F_2$, $Ca_5(PO_4)_3F$, Sr_3AlO_4F, $Sr_3NaLa(PO_4)_3F$, $Sr_3GdNa(PO_4)_3$, $Sr_5(BO_3)_3Cl$, $Ca_{5.45}Li_{3.55}(SiO_4)_3O_{0.45}F_{1.55}$, $Ba_2Ln(BO_3)_2Cl$ (Ln = Y, Gd or Lu), and $NaCa_2LuSi_2O_7F_2$.[26–40]

College of Physics Science and Technology, Hebei University, Baoding 071002, China. E-mail: li-panlai@126.com

† Electronic supplementary information (ESI) available. See DOI: 10.1039/c4tc01055h

In 1967 Greenblatt *et al.* reported the X-ray single crystal structure of Ca_2PO_4Cl, which crystallized in an orthorhombic system with space group pbcm(57) and with four formula units per unit cell ($Z = 4$).[41,42] The crystal structure consisted of discrete and distorted PO_4^{3-} tetrahedrons, held together primarily by Ca^{2+} ions. Two different crystallographic sites are available for the divalent Ca^{2+} ions, one with site symmetry C_2 and the other with site symmetry C_S. In both sites the Ca^{2+} is coordinated by six oxide and two chloride ions. In the larger site, the average Ca–O distance is about 0.250 nm and the average Ca–Cl distance 0.289 nm. For the smaller C_2 site, the corresponding distances are 0.246 nm and 0.281 nm, respectively.[41,42]

In the 1990s Blasse *et al.* investigated the luminescence and thermo-luminescence of Eu^{2+} in Ca_2PO_4Cl,[43] and Chen *et al.* determined the external quantum efficiency (QE) as 61% under excitation with 400 nm radiation.[44] Guo *et al.* studied the synthesis of $Ca_2PO_4Cl:Eu^{2+}$.[45] Based on the effective ionic radii (r) of cations with different coordination numbers (CN),[44] the ionic radius of Eu^{2+} (CN = 8, $r = 0.125$ nm) is close to that of Ca^{2+} (CN = 8, $r = 0.112$ nm). Because the four-coordinated P^{5+} ($r = 0.017$ nm) site is too small for Eu^{2+} to occupy, the Eu^{2+} is believed to occupy the larger Ca^{2+} sites.

The transition metal ion, Mn^{2+}, can exhibit a broad emission band in the visible range because of d–d transition, but this is forbidden and difficult to pump. Because an Eu^{2+} ion can act as a good sensitizer, transferring part of its energy to activator ions,[14–16] it is a promising sensitizer for Mn^{2+} ions, and Eu^{2+} can be used to improve the emission intensity of Mn^{2+} in a number of hosts.[14–16] Nevertheless, little attention has been given in the literature towards the luminescence of $Ca_2PO_4Cl:Eu^{2+}$, Mn^{2+}, despite its potential application in white LEDs. In the present investigation the luminescence and energy transfer of $Ca_2PO_4Cl:Eu^{2+}$, Mn^{2+} have been explored, and a warm, white emitting phosphor with low CCT has been achieved by varying the relative doping of Eu^{2+} and Mn^{2+}.

2. Experimental

2.1 Sample preparation

A series of samples of $Ca_{2-x-y}PO_4Cl:xEu^{2+}$, yMn^{2+} (x, y being molar concentrations) have been synthesized by a high temperature solid-state method. The initial materials, including Eu_2O_3 (99.99% purity), and analytical reagent quality $CaCO_3$, $CaCl_2 \cdot 6H_2O$, $NH_4H_2PO_4$ and $MnCO_3$, were thoroughly mixed in stoichiometric proportions and ground for more than 30 min in an agate pestle and mortar to ensure a completely uniform distribution. The mixtures obtained were heated at 1000 °C for 2 h in a reducing atmosphere (5% H_2:95% N_2), and then allowed to cool to room temperature. In order to measure their characteristics, the samples were again ground to powder. White LEDs were fabricated by integrating a mixture of transparent silicone resin and $Ca_2PO_4Cl:Eu^{2+}$, Mn^{2+} on a 400 nm LED chip.

2.2 Characterization of materials

Phase formation of the $Ca_{2-x-y}PO_4Cl:xEu^{2+}$, yMn^{2+} phosphors was carefully checked by powder X-ray diffraction (XRD; Bruker AXS D8 ADVANCE automatic diffractometer), with Ni-filtered Cu Kα_1 radiation ($\lambda = 0.15405$ nm) operating at 40 kV and 40 mA, and with a scan rate of 0.02° s^{-1} was applied to record the patterns in the range, $2\theta = 10°$ to 70°.

Room temperature photoluminescence spectra and luminescence decay curves were determined using a fluorescence spectrometer (Edinburgh Instruments FLS920) with a 450 W Xe lamp as excitation source, with a scanning wavelength from 200 to 700 nm and spectral resolution of 0.2 nm. The scanning time range was 0 to 5000 ns, with a time resolution of 10 ns, using a pulsed diode laser (Edinburgh Instruments EPL 375) as excitation source. Quantum efficiency was determined using a photoluminescence quantum efficiency measurement system (Hamamatsu Photonics C9920-02) using a 150 W Xe lamp. The measurements were conducted at room temperature. High-temperature photoluminescence spectra were determined on a fluorescence spectrophotometer (Hitachi F-4600) with a TAP-02 high-temperature control system, at a scanning wavelength range of 400–700 nm, a spectral resolution of 0.2 nm, and a 450 W Xe lamp as excitation source.

3. Results and discussion

3.1 Phase formation

XRD patterns of $Ca_2PO_4Cl:Eu^{2+}$, $Ca_2PO_4Cl:Mn^{2+}$, and $Ca_2PO_4Cl:Eu^{2+}$, Mn^2 were determined, and a similar diffraction pattern was observed for each sample. As a representative example, Fig. 1 shows the XRD pattern of $Ca_2PO_4Cl:0.07Eu^{2+}$, $Ca_2PO_4Cl:0.4Mn^{2+}$, $Ca_2PO_4Cl:0.07Eu^{2+}$, and $0.2Mn^{2+}$. When the diffraction data was compared with the standard JCPDS card (19-0247), the uniformity of diffraction patterns indicated that the phase formation of Ca_2PO_4Cl was not influenced by small amounts of either Eu^{2+}, Mn^{2+}, or Eu^{2+}/Mn^{2+}. However, as shown in Fig. 1, with larger quantities of impurity, such as $0.07Eu^{2+}$, the XRD pattern peaks were shifted slightly to smaller angles. For Mn^{2+}-doped Ca_2PO_4Cl, the XRD pattern peaks were slightly shifted to larger angles. According to Vegard's law, the ionic size of the Eu^{2+} (Mn^{2+}) ion is bigger (smaller) than that of the Ca^{2+} ion, so this is reasonable. Ca_2PO_4Cl crystallizes in the

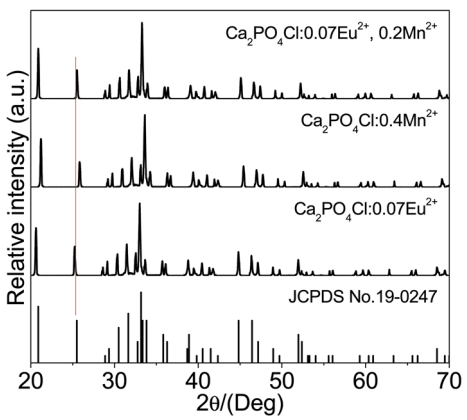

Fig. 1 XRD patterns of $Ca_2PO_4Cl:0.07Eu^{2+}$, $Ca_2PO_4Cl:0.4Mn^{2+}$ and $Ca_2PO_4Cl:0.07Eu^{2+}$, $0.2Mn^{2+}$.

orthorhombic system with space group pbcm(57) and with four formula units per unit cell ($N = 4$), and the dimensions of a unit cell are $a = 0.6185$ nm, $b = 0.6983$ nm and $c = 1.082$ nm.

3.2 Luminescence properties of Eu^{2+} and Mn^{2+} in Ca_2PO_4Cl

Fig. 2(a) shows that, under 370 nm radiation excitation, Ca_2PO_4Cl:0.07Eu^{2+} had a broad emission band, the peak being located at 450 nm, which is typically attributed to the $4f^65d^1 \rightarrow 4f^7$ electronic dipole-allowed transition of the Eu^{2+} ion. Two different crystallographic sites are available for the divalent Ca^{2+} ions, one with site symmetry C_2 and the other with site symmetry C_S, and thus, Eu^{2+} ions may occupy either of the two sites.[44] The excitation spectrum consists mainly of an unresolved band, because of the $4f^7 \rightarrow 4f^65d^1$ transition of the Eu^{2+} ion. When Eu^{2+} ions occupy the lattice sites with C_2 or C_S symmetry in Ca_2PO_4Cl, a five-fold degeneracy of 5d levels is expected in the excitation spectrum. Furthermore, the dominating bands in the excitation spectrum are difficult to resolve because of the pronounced overlap between the 5d levels. The broad excitation band may be ascribed to the high covalency of the Ca_{Eu}–Cl bonding and large crystal-field splitting. The inset in Fig. 2(a) shows the emission spectra of Ca_2PO_4Cl:$x$$Eu^{2+}$ at different Eu^{2+} concentrations, in which the spectral distribution has a similar shape, regardless of Eu^{2+} concentration. However, the emission intensity is influenced by Eu^{2+} concentration, and the optimal concentration is seen to be located at $x = 0.07$.

Fig. 2(b) shows that Ca_2PO_4Cl:0.4Mn^{2+} had a broadband orange-red emission around 591 nm, ascribed to the spin-forbidden $^4T_1(^4G)$–$^6A_1(^6S)$ transition of the Mn^{2+} ion. The excitation spectrum of Ca_2PO_4Cl:Mn^{2+} contains a number of bands, and the strongest excitation at 405 nm corresponds to the transition from the $^6A_1(^6S)$ ground state to the excited states [^4E (^4G), $^4A_1(^4G)$].[14–16] The emission spectra of Ca_2PO_4Cl:$y$$Mn^{2+}$ are shown in the inset of Fig. 2(b) at different Mn^{2+} concentrations (y). The emission intensities increased with increasing Mn^{2+} concentration, reaching a maximum at 0.4 Mn^{2+}, then decreasing because of concentration quenching.

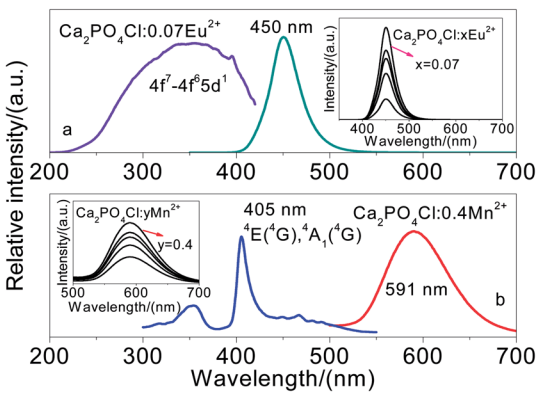

Fig. 2 Emission and excitation spectra of (a) Ca_2PO_4Cl:0.07Eu^{2+} (λ_{ex} = 370 nm) and (b) Ca_2PO_4Cl:0.4Mn^{2+} (λ_{ex} = 405 nm). Inset: (a) emission spectrum of Ca_2PO_4Cl:$x$$Eu^{2+}$ (λ_{ex} = 370 nm) at different Eu^{2+} concentrations (x); (b) emission spectrum of Ca_2PO_4Cl:$y$$Mn^{2+}$ (λ_{ex} = 405 nm) at different Mn^{2+} concentrations (y).

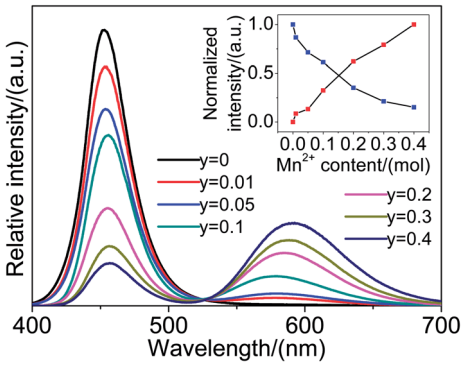

Fig. 3 Emission spectra of Ca_2PO_4Cl:0.07Eu^{2+}, $y$$Mn^{2+}$ (λ_{ex} = 370 nm).

3.3 Luminescent properties and energy transfer of $Eu^{2+} \rightarrow Mn^{2+}$ in Ca_2PO_4Cl

As shown in Fig. 2, there was an obvious spectral overlap between the emission spectra of Eu^{2+} and Mn^{2+}, indicating the possibility of energy transfer from Eu^{2+} to Mn^{2+} in Ca_2PO_4Cl. In order to investigate the luminescence and this energy transfer, a series of Ca_2PO_4Cl:Eu^{2+}, Mn^{2+} samples were synthesized and their luminescence systematically investigated. Fig. 3 shows the emission spectra of Ca_2PO_4Cl:0.07Eu^{2+}, $y$$Mn^{2+}$ (y = 0–0.4) under 370 nm radiation excitation. These consisted of both a broad blue and an orange-red emission band. The broad blue emission band from 400 to 525 nm is typically attributed to the $4f^65d^1 \rightarrow 4f^7$ electronic dipole-allowed transition of the Eu^{2+} ion, whereas the orange-red emission band from 525 to 700 nm is attributed to the $^4T_1$–$^6A_1$ forbidden transition of Mn^{2+}. Emission intensities of Eu^{2+} were found to decrease monotonically with increasing Mn^{2+} concentration, whereas the emission intensities of Mn^{2+} reached a maximum at $y = 0.4$.

Inset: normalized intensity of Eu^{2+} and Mn^{2+} as a function of Mn^{2+} concentration (λ_{ex} = 370 nm).

In order to study the energy transfer from Eu^{2+} to Mn^{2+}, the normalized intensities of Eu^{2+} and Mn^{2+} in Ca_2PO_4Cl were recorded and are shown in the inset of Fig. 3. This shows that the emission intensity of Eu^{2+} decreased, and that of Mn^{2+} gradually increased, with increasing Mn^{2+} concentration. These results indicate that an efficient energy transfer of $Eu^{2+} \rightarrow Mn^{2+}$ was taking place in Ca_2PO_4Cl:Eu^{2+}, Mn^{2+}.

For the blue and orange-red emission of Ca_2PO_4Cl:0.07Eu^{2+}, $y$$Mn^{2+}$, the corresponding excitation spectra are shown in Fig. 4. It is clear that similar excitation characteristics of Eu^{2+} are present at different Mn^{2+} concentrations, which also confirms the energy transfer from Eu^{2+} to Mn^{2+}.

In order to properly understand the energy transfer process, the energy transfer efficiency (η_T) of the phosphors from Eu^{2+} to Mn^{2+} was calculated. According to Paulose *et al.*[46] η_T can be expressed as in eqn (1):

$$\eta_T = 1 - (I_S/I_{S0}) \approx 1 - (\tau_S/\tau_{S0}), \quad (1)$$

where I_{S0} and I_S are the luminescence intensities of sensitizer Eu^{2+} in the absence and presence of activator Mn^{2+}, respectively, and where τ_{S0} and τ_S are the decay lifetimes of the sensitizer

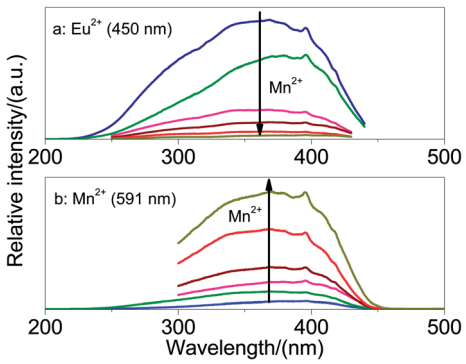

Fig. 4 Excitation spectra of Ca_2PO_4Cl:0.07Eu^{2+}, yMn^{2+} (a) λ_{em} = 450 nm, and (b) λ_{em} = 591 nm.

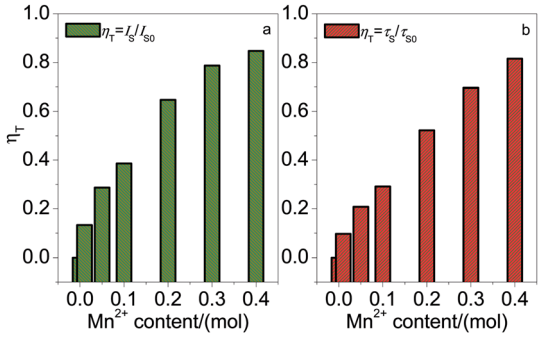

Fig. 5 Variation in η_T for Ca_2PO_4Cl:0.07Eu^{2+}, yMn^{2+} (y = 0–0.4) with Mn^{2+} concentration, (a) $\eta_T = 1 - (I_S/I_{S0})$, and (b) $\eta_T = 1 - (\tau_S/\tau_{S0})$.

Eu^{2+} in the absence and presence of activator Mn^{2+}. As shown in Fig. 3, the emission intensities (I_S and I_{S0}) can be obtained, and the η_T values (the dark yellow patterns) from Eu^{2+} to Mn^{2+} for Ca_2PO_4Cl:Eu^{2+}, yMn^{2+} (y = 0–0.4) calculated, and these are shown in Fig. 5(a).

In order to achieve decay lifetimes, the fluorescence lifetimes, τ, were measured for Eu^{2+} at different Mn^{2+} concentrations. As a representative example, Fig. 6 shows the results of Ca_2PO_4Cl:Eu^{2+}, yMn^{2+} (y = 0, 0.1, 0.2 and 0.3) (λ_{ex} = 375 nm, λ_{em} = 450 nm). The decay curves fit well with a second-order exponential decay mode, according to eqn (2):[11,14,39]

$$I = A_1 \exp(-t/\tau_1) + A_2 \exp(-t/\tau_2), \quad (2)$$

Where: I is the luminescence intensity; A_1 and A_2 are constants; t is time, and τ_1 and τ_2 are lifetimes for rapid and slow decay, respectively. Average lifetimes (τ*) can be obtained from eqn (3):[32–34]

$$\tau^* = (A_1\tau_1^2 + A_2\tau_2^2)/(A_1\tau_1 + A_2\tau_2) \quad (3)$$

For Ca_2PO_4Cl:Eu^{2+}, yMn^{2+} (y = 0–0.4), the calculated average lifetimes (τ*) are 664.2, 600.0, 526.2, 470.7, 317.2, 201.9 and 122.6 ns, respectively. According to the results, the energy transfer efficiency (η_T) may be calculated using eqn (1), and the η_T value can be seen from the red bars in Fig. 5(b). The results show the close agreement between the use of intensity and decay time. The energy transfer efficiency from Eu^{2+} to Mn^{2+} gradually increases with increasing Mn^{2+} concentration. At a concentration of 0.4 mol Mn^{2+}, the energy transfer efficiency is above 82.0%.

On the basis of the Dexter energy transfer formula for exchange and multipolar interactions, the following relationships can be calculated:[47–50]

$$\ln(\eta_0/\eta) \propto C \quad (4)$$

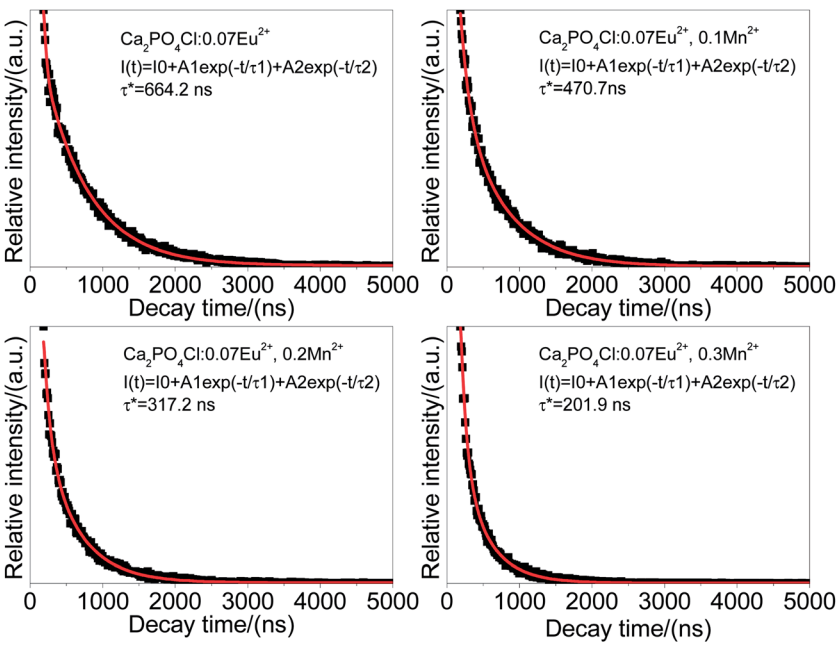

Fig. 6 Decay curves of Eu^{2+} emission monitored at 450 nm for Ca_2PO_4Cl:0.07Eu^{2+}, yMn^{2+} (λ_{ex} = 375 nm).

$$(\eta_0/\eta) \propto C^{\alpha/3}, \quad (5)$$

where η_0 and η are the luminescence QE of Eu^{2+} in the absence and presence of Mn^{2+}, respectively, and C is the total concentration of Eu^{2+} and Mn^{2+}. Eqn (4) corresponds to the exchange interaction, and eqn (5) with $\alpha = 6$, 8 or 10 corresponds to dipole–dipole, dipole–quadrupole, and quadrupole–quadrupole interactions, respectively. The value of η_0/η can be estimated approximately from the correlated lifetime ratio (τ_{S0}/τ_S), thus, eqn (4) and (5) can be changed as follows:

$$\ln(\tau_{S0}/\tau_S) \propto C \quad (6)$$

$$(\tau_{S0}/\tau_S) \propto C^{\alpha/3} \quad (7)$$

The relationship between $\ln(\tau_{S0}/\tau_S) \propto C$ and $(\tau_{S0}/\tau_S) \propto C^{\alpha/3}$ is illustrated in Fig. 7. By examination of the fitting factor R, the relationship $(\tau_{S0}/\tau_S) \propto C^{8/3}$ gives the best fitting, implying that the dipole–quadrupole interaction is applicable to the energy transfer from Eu^{2+} to Mn^{2+}.

In general, the critical distance (R_c) can be calculated using a concentration quenching method. The critical distance R_{Eu-Mn} between Eu^{2+} and Mn^{2+} can be estimated by eqn (8):[51]

$$R_{Eu-Mn} = 2[3V/(4\pi x_c N)]^{1/3}, \quad (8)$$

Where: x is the total concentration of Eu^{2+} and Mn^{2+}, N is number of Z ions in the unit cell (for Ca_2PO_4Cl, $N = 4$), and V is the volume of the unit cell (for Ca_2PO_4Cl, $V = 0.46731$ nm^3). The estimated distance (R_{Eu-Mn}) for Ca_2PO_4Cl:0.07Eu^{2+}, $y$$Mn^{2+}$ phosphors (x_c = 0.07, 0.08, 0.12, 0.17, 0.27, 0.37, and 0.47) are 1.47, 1.41, 1.23, 1.09, 0.94, 0.84 and 0.78 nm, respectively. The distances between Eu^{2+} and Mn^{2+} become shorter with increasing Mn^{2+} concentration, and x is the critical concentration at which the emission intensity of the donor (Eu^{2+}) in the presence of the acceptor (Mn^{2+}) is half that in the absence of the acceptor (Mn^{2+}). Thus, the critical distance (R_c) of the energy transfer is calculated to be about 1.09 nm for Ca_2PO_4-Cl:0.07Eu^{2+}, $y$$Mn^{2+}$. R_{Eu-Mn} for various Eu^{2+} contents is much larger than the typical critical distance for exchange interaction (0.5 nm).[52]

These results indicate that the exchange interaction plays no role in the energy transfer process for Ca_2PO_4Cl:0.07Eu^{2+}, $y$$Mn^{2+}$. The emission intensities of Mn^{2+}, are therefore, obviously enhanced by the efficient energy transfer from Eu^{2+} to Mn^{2+}, which is part of the multipolar interaction.

3.4 CIE coordinates, thermal stability and quantum efficiency of $Ca_2PO_4Cl:Eu^{2+}$, Mn^{2+}

Color coordinates are an important factor in evaluating the performance of phosphors. As shown in Fig. 8 and Table S1,† the Commission Internationale de l'Eclairage (CIE) chromaticity coordinates and CCT of Ca_2PO_4Cl:0.07Eu^{2+}, $y$$Mn^{2+}$ were measured. While the concentration of Mn^{2+} increased from zero to 0.4, the Eu^{2+} concentration was fixed at 0.07. The corresponding color of the phosphor shifted from blue to white light, and eventually to orange-red. In particular, the CCT of white light can be tuned by appropriate changes in Mn^{2+} concentration. It is evident that warm, white light can be produced for different practical applications by varying the Mn^{2+} concentration in $Ca_2PO_4Cl:Eu^{2+}$, Mn^{2+}.

For the application of high power LEDs, the thermal stability of the phosphor is an important issue. For Ca_2PO_4Cl:0.07Eu^{2+}, $y$$Mn^{2+}$, the temperature dependence of the emission spectra under 370 nm radiation excitation is shown in Fig. 9. The inset illustrates the temperature quenching characteristics of commercial YAG:Ce and a typical sample, Ca_2PO_4Cl:0.07Eu^{2+}, 0.2Mn^{2+}, within the temperature range 20–250 °C. When the temperature is raised to 200 °C, the emission intensity of Ca_2-PO_4Cl:0.07Eu^{2+}, 0.2Mn^{2+} becomes very close to that of YAG:Ce;

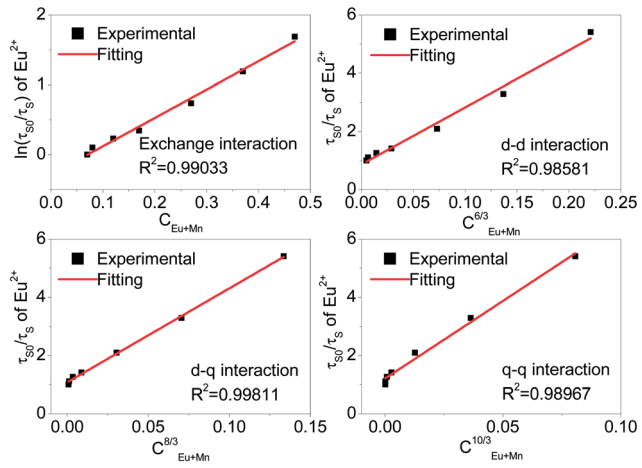

Fig. 7 Dependence of $\ln(\tau_{S0}/\tau_S)$ of Eu^{2+} on (a) C and τ_{S0}/τ_S of Eu^{2+} on (b) $C^{6/3}$, (c) $C^{8/3}$, and (d) $C^{10/3}$.

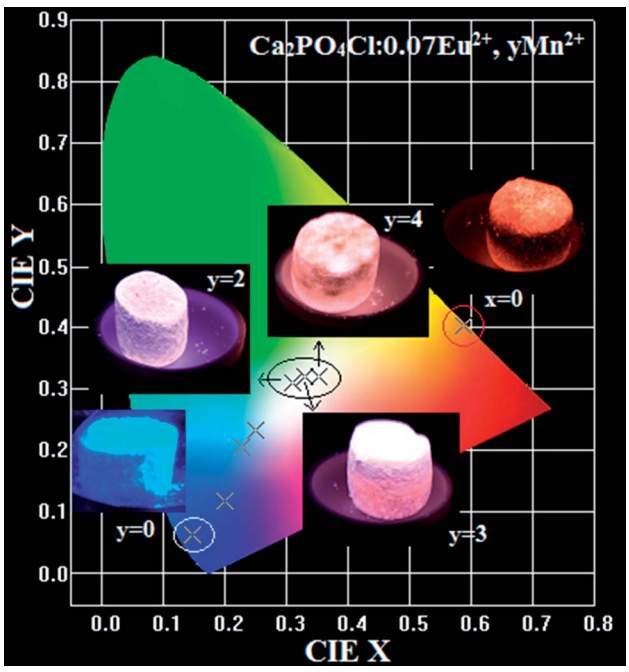

Fig. 8 CIE chromaticity coordinates and the corresponding luminescence of Ca_2PO_4Cl:0.07Eu^{2+}, $y$$Mn^{2+}$ (y = 0–0.4; λ_{ex} = 365 nm).

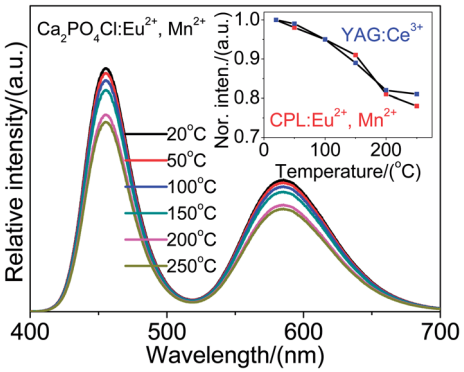

Fig. 9 Temperature-dependent emission spectra of Ca_2PO_4Cl:0.07Eu^{2+}, 0.2Mn^{2+} (λ_{ex} = 370 nm). Inset: normalized intensity of Ca_2PO_4Cl:0.07Eu^{2+}, 0.2Mn^{2+} and YAG:Ce as a function of temperature.

and, for example, the intensity of the sample drops to about 81% at this temperature, whereas that of YAG:Ce decreases to 82% of its initial value. These results obviously indicate that the sample also has good thermal quenching properties.

In the application of white LEDs, QE is an important parameter in LED phosphors. In general, a tunable white light emission with a suitable QE can be obtained in Ca_2PO_4Cl:0.07Eu^{2+}, yMn^{2+} by efficient energy transfer from Eu^{2+} to Mn^{2+} ions, as shown in Table S1.† For the warm, white light-emitting phosphor Ca_2PO_4Cl:0.07Eu^{2+}, 0.2Mn^{2+}, QE can reach 59.6%. These data indicate that this light-emitting phosphor has the appropriate QE and warm white light emission, and it could, therefore, be used as a phosphor for white LEDs.

3.5 Spectrum of white LEDs fabricated with $Ca_2PO_4Cl:Eu^{2+}$, Mn^{2+}

To demonstrate the potential application of $Ca_2PO_4Cl:Eu^{2+}$, Mn^{2+}, a white LED was fabricated by coating a Ca_2PO_4Cl:0.07Eu^{2+}, 0.2Mn^{2+} phosphor on to a 400 nm UV-chip driven by a 350 mA current. The emission spectrum of white LEDs is represented in Fig. 10, which has CIE color coordinates (0.3102, 0.3096), a CCT of 4296 K, and color rendering index (R_a) of 86. The results demonstrate that the performance of white LEDs based on the Ca_2PO_4Cl:0.07Eu^{2+}, 0.2Mn^{2+} phosphor is superior to that of white LEDs prepared by coating a YAG:Ce yellow phosphor on blue chips [CIE (0.292, 0.325), CCT = 7756 K], because it shows both a higher color rendering index and a lower CCT value.[4]

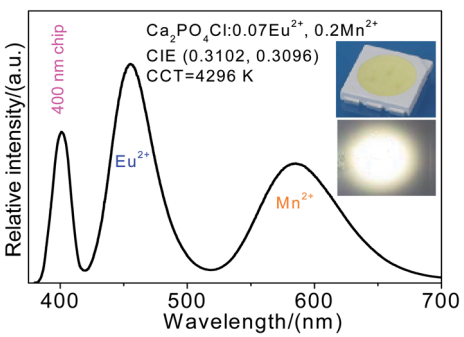

Fig. 10 Emission spectrum of a phosphor-converted LED (pc-LED) lamp fabricated with a 400 nm LED chip and warm, white-emitting phosphor Ca_2PO_4Cl:0.07Eu^{2+}, 0.2Mn^{2+}.

The inset shows the appearance of a well-packaged trichromatic LED lamp in operation.

4. Conclusions

$Ca_2PO_4Cl:Eu^{2+}$, Mn^{2+} can be excited by *n*-UV excitation, and the corresponding color of the phosphor can shift from blue to white light, and eventually to orange-red, by the efficient resonant energy transfer from Eu^{2+} to Mn^{2+} ions in Ca_2PO_4Cl. In particular, a warm white emission phosphor can be realized by combining the emission of Eu^{2+} and Mn^{2+} in Ca_2PO_4Cl. The energy transfer efficiency increases with increasing Mn^{2+} content, and the dipole–quadrupole interaction is applicable in the energy transfer from Eu^{2+} to Mn^{2+}. A warm, white LED may be fabricated using the warm, white-emitting phosphor Ca_2PO_4Cl:0.07Eu^{2+}, 0.2Mn^{2+} pumped by a 400 nm LED-chip with good CIE coordinates (0.3102, 0.3096), lower CCT (4296 K) and a high color rendering index (R_a) of 86. Thus, $Ca_2PO_4Cl:Eu^{2+}$, Mn^{2+} can potentially serve as a light-emitting phosphor for white LEDs.

Acknowledgements

The study was supported by the National Natural Science Foundation of China (50902042), the Natural Science Foundation of Hebei Province, China (A2014201035 and E2014201037) and the Education Office Research Foundation of Hebei Province, China (ZD2014036 and QN2014085).

References

1 M. Shang, C. Li and J. Lin, *Chem. Soc. Rev.*, 2014, **43**, 1372.
2 C. C. Lin and R.-S. Liu, *J. Phys. Chem. Lett.*, 2011, **2**, 1268.
3 S. Ye, F. Xiao, Y. X. Pan, Y. Y. Ma and Q. Y. Zhang, *Mater. Sci. Eng., R*, 2010, **71**, 1.
4 C.-W. Yeh, W.-T. Chen, R.-S. Liu, S.-F. Hu, H.-S. Sheu, J.-M. Chen and H. T. Hintzen, *J. Am. Chem. Soc.*, 2012, **134**, 14108.
5 J. Hou, W. Jiang, Y. Fang and F. Huang, *J. Mater. Chem. C*, 2013, **1**, 5892.
6 Z. Wang, P. Li, Q. Guo and Z. Yang, *Mater. Res. Bull.*, 2014, **52**, 30.
7 C. Zhang, S. Huang, D. Yang, X. Kang, M. Shang, C. Peng and J. Lin, *J. Mater. Chem.*, 2010, **20**, 6674.
8 C.-H. Huang, T.-S. Chan, W.-R. Liu, D.-Y. Wang, Y.-C. Chiu, Y.-T. Yeh and T.-M. Chen, *J. Mater. Chem.*, 2012, **22**, 20210.
9 H. Liu, Y. Luo, Z. Mao, L. Liao and Z. Xia, *J. Mater. Chem. C*, 2014, **2**, 1619.
10 W. Lü, Z. Hao, X. Zhang, Y. Luo, X. Wang and J. Zhang, *Inorg. Chem.*, 2011, **50**, 7846.
11 C.-H. Huang and T.-M. Chen, *J. Phys. Chem. C*, 2011, **115**, 2349.

12 X. M. Liu, C. K. Lin and J. Lin, *Appl. Phys. Lett.*, 2007, **90**, 081904.
13 C. C. Chang and T.-M. Chen, *Appl. Phys. Lett.*, 2007, **91**, 081902.
14 C.-H. Huang, T.-M. Chen, W.-R. Liu, Y.-C. Chiu, Y.-T. Yeh and S.-M. Jang, *ACS Appl. Mater. Interfaces*, 2010, **2**, 259.
15 W.-R. Liu, C.-H. Huang, C.-W. Yeh, J.-C. Tsai, Y.-C. Chiu, Y.-T. Yeh and R.-S. Liu, *Inorg. Chem.*, 2012, **51**, 9636.
16 W.-R. Liu, C.-H. Huang, C.-W. Yeh, Y.-C. Chiu, Y. T. Yeh and R.-S. Liu, *RSC Adv.*, 2013, **3**, 9023.
17 G. Li, Y. Zhang, D. Geng, M. Shang, C. Peng, Z. Cheng and J. Lin, *ACS Appl. Mater. Interfaces*, 2012, **4**, 296.
18 G. Li, D. Geng, M. Shang, Y. Zhang, C. Peng, Z. Cheng and J. Lin, *J. Phys. Chem. C*, 2011, **115**, 21882.
19 D. Geng, M. Shang, Y. Zhang, H. Lian, Z. Cheng and J. Lin, *J. Mater. Chem. C*, 2013, **1**, 2345.
20 Y. Zhang, G. Li, D. Geng, M. Shang, C. Peng and J. Lin, *Inorg. Chem.*, 2012, **51**, 11655.
21 N. Guo, Y. Zheng, Y. Jia, H. Qiao and H. You, *J. Phys. Chem. C*, 2012, **116**, 1329.
22 G. Zhu, S. Xin, Y. Wen, Q. Wang, M. Que and Y. Wang, *RSC Adv.*, 2013, **3**, 9311.
23 N. Guo, Y. Jia, W. Lü, W. Lv, Q. Zhao, M. Jiao, B. Shao and H. You, *Dalton Trans.*, 2013, **42**, 5649.
24 W. Li, R.-J. Xie, T. Zhou, L. Liu and Y. Zhu, *Dalton Trans.*, 2014, **43**, 6132.
25 W.-T. Chen, H.-S. Sheu, R.-S. Liu and J. P. Attfield, *J. Am. Chem. Soc.*, 2012, **134**, 8022.
26 Q. Guo, L. Liao and Z. Xia, *J. Lumin.*, 2014, **145**, 65.
27 Z. Xia and R.-S. Liu, *J. Phys. Chem. C*, 2012, **116**, 15604.
28 L. Huang, M. Guo, S. Zhao, D. Deng, H. Wang, Y. Hua, G. Jia and S. Xu, *ECS J. Solid State Sci. Technol.*, 2013, **2**, R3083.
29 Z. Fu, X. Wang, Y. Yang, Z. Wu, D. Duan and X. Fu, *Dalton Trans.*, 2014, **43**, 2819.
30 L. Ning, Y. Wang, Z. Wang, W. Jin, S. Huang, C. Duan, Y. Zhang, W. Chen and H. Liang, *J. Phys. Chem. A*, 2014, **118**, 986.
31 S. Hu and W. Tang, *J. Lumin.*, 2014, **145**, 100.
32 R. Yu, H. M. Noh, B. K. Moon, B. C. Choi, J. H. Jeong, K. Jang, H. S. Lee and S. S. Yi, *Mater. Res. Bull.*, 2014, **51**, 361.
33 Z. Xia, J. Zhuang and L. Liao, *Inorg. Chem.*, 2012, **51**, 7202.
34 Z. Xia, J. Zhuang, A. Meijerink and X. Jing, *Dalton Trans.*, 2013, **42**, 6327.
35 J. Zhou, Z. Xia, M. Yang and K. Shen, *J. Mater. Chem.*, 2012, **22**, 21935.
36 Z. Xia, R.-S. Liu, K.-W. Huang and V. Drozd, *J. Mater. Chem.*, 2012, **22**, 15183.
37 Z. Xia, X. Wang, Y. Wang, L. Liao and X. Jing, *Inorg. Chem.*, 2011, **50**, 10134.
38 M. Jiao, Y. Jia, W. Lü, W. Lv, Q. Zhao, B. Shao and H. You, *J. Mater. Chem. C*, 2014, **2**, 90.
39 W. Lv, W. Lü, N. Guo, Y. Jia, Q. Zhao, M. Jiao, B. Shao and H. You, *Dalton Trans.*, 2013, **42**, 13071.
40 W. Lv, W. Lü, N. Guo, Y. Jia, Q. Zhao, M. Jiao, B. Shao and H. You, *RSC Adv.*, 2013, **3**, 16034.
41 M. Greenblatt, E. Banks and B. Post, *Acta Crystallogr.*, 1967, **23**, 166.
42 M. Greenblatt, E. Banks and B. Post, *Acta Crystallogr., Sect. B: Struct. Crystallogr. Cryst. Chem.*, 1969, **25**, 2170.
43 A. Meijering and G. Blasse, *J. Phys.: Condens. Matter*, 1990, **2**, 3619.
44 Y.-C. Chiu, W.-W. Liu, C.-K. Chang, C.-C. Liao, Y.-T. Yeh, S.-M. Jang and T.-M. Chen, *J. Mater. Chem.*, 2010, **20**, 1755.
45 R. Yu, C. Guo, T. Li and Y. Xu, *Curr. Appl. Phys.*, 2013, **13**, 880.
46 P. I. Paulose, G. Jose, V. Thomas, N. V. Unnikrishnan and M. K. R. Warrier, *J. Phys. Chem. Solids*, 2003, **64**, 841.
47 D. L. Dexter and J. H. Schulman, *J. Chem. Phys.*, 1954, **22**, 1063.
48 R. Reisfeld, E. Greenberg, R. Velapoldi and B. Barnett, *J. Chem. Phys.*, 1972, **56**, 1698.
49 U. Caldiño, J. L. Hernández-Pozos, C. Flores, A. Speghini and M. Bettinelli, *J. Phys.: Condens. Matter*, 2005, **17**, 7297.
50 R. Martínez-Martínez, M. García, A. Speghini, M. Bettinelli, C. Falcony and U. Caldiño, *J. Phys.: Condens. Matter*, 2008, **20**, 395205.
51 G. Blass, *Philips Res. Rep.*, 1969, **24**, 131.
52 G. Blasse and B. C. Grabmaier, *Luminescent Materials*, Berlin, Springer, 1994.